Revealing weak spin-orbit coupling effects on charge carriers in a π-conjugated polymer

H. Malissa,[1,*] R. Miller,[1] D. L. Baird,[1] S. Jamali,[1] G. Joshi,[1] M. Bursch,[2] S. Grimme,[2] J. van Tol,[3]
J. M. Lupton,[1,4] and C. Boehme[1]

[1]*Department of Physics and Astronomy, University of Utah, Salt Lake City, Utah 84112, USA*
[2]*Mulliken Center for Theoretical Chemistry, Institut für Physikalische und Theoretische Chemie, Universität Bonn, 53113 Bonn, Germany*
[3]*National High Magnetic Field Laboratory, Florida State University, Tallahassee, Florida 32310, USA*
[4]*Institut für Experimentelle und Angewandte Physik, Universität Regensburg, Universitätsstrasse 31, 93053 Regensburg, Germany*

We measure electrically detected magnetic resonance on organic light-emitting diodes made of the polymer poly[2-methoxy-5-(2-ethylhexyloxy)-1,4-phenylenevinylene] at room temperature and high magnetic fields where spectral broadening of the resonance due to spin-orbit coupling (SOC) exceeds that due to the local hyperfine fields. Density-functional-theory calculations on an open-shell model of the material reveal g-tensors of charge-carrier spins in the lowest unoccupied (electron) and highest occupied (hole) molecular orbitals. These tensors are used for simulations of magnetic resonance line shapes. Besides providing the first quantification and direct observation of SOC effects on charge-carrier states in these weakly SO-coupled hydrocarbons, this procedure demonstrates that spin-related phenomena in these materials are fundamentally monomolecular in nature.

Charge-carrier states of hydrocarbon-based materials, such as π-conjugated polymer films, are known to exhibit very weak spin-orbit coupling (SOC) compared to many other compounds [1–7]. For the description of some of these materials' physical behavior, including their magnetoresistance, luminescence, and permeability [1,8–10], it is a reasonable assumption to consider SOC to be negligible [5]. In contrast to this, however, there are other material properties, such as high-field magneto-optoelectronic characteristics [11,12], spin lifetimes [12,13], spin-diffusion lengths [1,4], the inverse spin-Hall effect [14–17], or the general spin statistics of organic light-emitting diodes (OLEDs), which determine overall OLED efficiency, where this assumption leads to incorrect predictions. Furthermore, the study of the influence of SOC on paramagnetic states—i.e., on polarons—such as g-factor shifts and anisotropies opens up a route for scrutinizing theoretical predictions of the nature of these states. Quantum chemistry is used to calculate energy levels by computing the carrier wave functions. The quality of these calculations can be tested by examining the g-tensors computed by density-functional-theory (DFT) methods. There have been recent material studies which specifically aim at the investigation and control of SOC in organic semiconductors [18]. However, these studies are based on doping with heavy elements, which induce strong SOC, and are only peripherally of relevance to OLEDs since they are carried out in solution.

In the following we investigate the effects of SOC on the Landé g-factors [19] of charge carriers in low-lying electronic cationic and anionic states [as approximated by the lowest unoccupied molecular orbital (LUMO) and the highest occupied molecular orbital (HOMO), respectively] containing

mobile electrons or holes, in the π-conjugated polymer poly[2-methoxy-5-(2-ethylhexyloxy)-1,4-phenylenevinylene] (MEH-PPV). We consider thin films of the material in OLED devices under room-temperature bipolar charge-carrier injection conditions. The experimental approach taken here is based on the shifts and broadening of magnetic resonance spectra, which arise due to the influence of SOC on the g-factor. Since MEH-PPV consists of relatively light elements (C, H, and O), SOC is weak and g-factors are therefore close to the free-electron value of 2.002 319 [20–22]. However, because even weak SOC leads to a minuscule g-factor shift and gives rise to spectroscopic fingerprints, such as an anisotropic g-tensor, it becomes detectable in magnetic-resonance spectroscopy at large B_0 fields, i.e., at large Zeeman splitting of the spin levels. To detect SOC effects in magnetic resonance, the spectral broadening induced by SOC must exceed that arising from local hyperfine fields due to hydrogen nuclei [20,23,24].

We therefore use high-magnetic-field [25] electrically detected magnetic resonance spectroscopy (EDMR), which enables the measurement of charge-carrier (polaron) pair magnetic resonance spectra of electrons and holes by recording spin-dependent charge carrier recombination currents in OLEDs [20–22,24,26]. We note that extensive previous work has demonstrated that the resonant species are indeed weakly spin-spin-coupled $S = \frac{1}{2}$ carriers [22,23,27]. This information derives from time-resolved measurements of the Rabi precession frequency [22,23]. The minuscule zero-field splitting of the carrier pair corresponds to fields of approximately 100 nT [27] and is therefore entirely irrelevant for the high-field experiments discussed here. We have discussed technical details of low-field EDMR experiments on such devices in detail previously [20,21,28], but all these reports pertained to EDMR experiments below fields of 1 T. Under these low-field
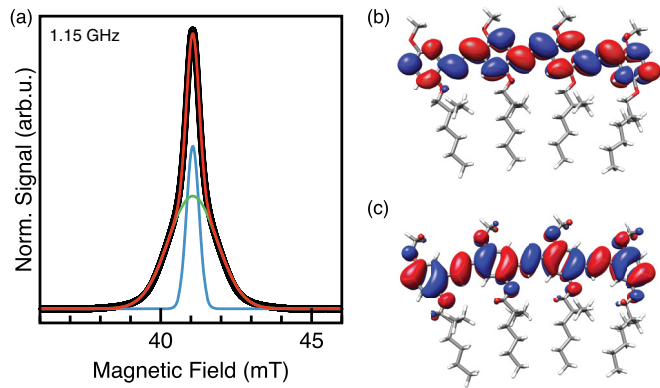
*hans.malissa@utah.edu

FIG. 1. (a) Room-temperature EDMR spectrum of MEH-PPV with a double-Gaussian fit (red). (b) and (c) Plots of the single-carrier probability density in the (b) LUMO and (c) HOMO of a model of MEH-PPV.
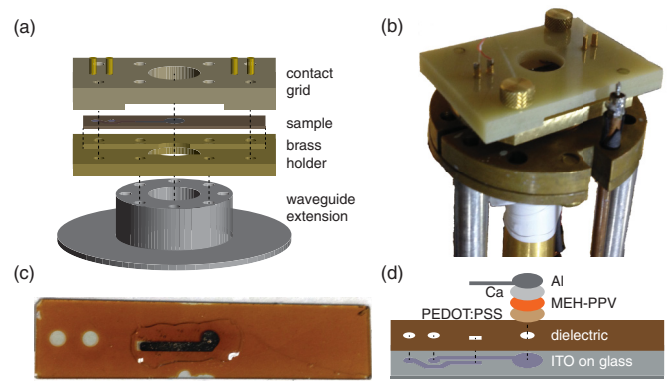

FIG. 2. (a) Sketch of the high-magnetic-field EDMR probe head. (b) Photograph of the probe head when mounted to the waveguide. (c) The OLED sample for high-field EDMR. (d) Sketch of the sample design (the encapsulation is omitted).

conditions, g-factor distributions in MEH-PPV due to weak SOC are spectroscopically detectable only qualitatively above fields of 300 mT in the form of a magnetic-field-dependent spectral broadening [20]. However, on an absolute scale, at these low fields, SOC effects are negligible compared to the contributions to the resonance spectrum from strong hyperfine-field distributions of the omnipresent hydrogen nuclei. Figure 1(a) shows an EDMR spectrum of a MEH-PPV OLED measured at a microwave (MW) frequency of 1.15 GHz using B_0 modulation and lock-in detection (cf. Ref. [20] and the Supplemental Material [29]). Note that the data displayed represent the integrated signal. At this low MW frequency, the linewidths of electron and hole resonances are governed solely by the hyperfine coupling with surrounding hydrogen nuclei, which give rise to Gaussian disorder broadening. The observed spectra can therefore be modeled by a superposition of two Gaussian lines with identical line centers, i.e., with effective g-factors of free electrons, but with two different linewidths. From the fit shown in Fig. 1(a), spectral widths of 0.208 and 0.811 mT are obtained, which provide a quantification of the distribution in hyperfine-field strengths experienced by each carrier of the pair.

In contrast to the data of Fig. 1(a), the high-field EDMR experiments reported here allow us to resolve shifts in the g-factor of the charge-carrier spins probed arising due to the small but finite SOC [30]. These shifts become relevant on magnetic-field scales which significantly exceed the magnetic-field range of hyperfine broadening. In particular, high-field EDMR measurements reveal anisotropic g-tensors which, together with the random spatial orientation of orbitals within the ensembles, give rise to asymmetries in the resonance lines.

In order to interpret the experimental results, we conducted DFT quantum-chemical calculations on a spin-polarized open-shell ($S = \frac{1}{2}$) model of the material by using molecular structures consisting of four monomer units of MEH-PPV with either an electron added (MEH-PPV$^-$) or an electron removed (MEH-PPV$^+$) (see the Supplemental Material [29]). The structures were optimized in the gas phase at the TPSSh-D3(BJ)/def2-TZVP [31–36] level of theory using the TURBO-MOLE program package [37,38]. The computed MOs of the electron (LUMO) and hole (HOMO) based on the optimized

structures are shown in Figs. 1(b) and 1(c) [39]. DFT calculations further yield electronic g-tensors for both model systems at the TPSSh/IGLO-III/TPSSh-D3(BJ)/def2-TZVP [40] level of theory provided by the ORCA program package [41].

EDMR experiments at very high MW frequencies (see the Supplemental Material [29] and Refs. [30,42]) were carried out using a 120-, 240-, and 336-GHz multifrequency quasioptical heterodyne electron paramagnetic resonance spectrometer at the National High Magnetic Field Laboratory of Florida State University [25]. In this setup, the sample is irradiated with millimeter waves while mounted at the end of a corrugated waveguide. We developed a sample holder which allows for electrical connection to the OLED while meeting the geometrical requirements of the spectrometer's waveguide structures. The sample and sample-holder designs are shown in Fig. 2. Figure 2(a) sketches the sample holder which encompasses a waveguide extension and mounting flange, a brass plate with a rectangular pocket to accommodate the sample, and a bore hole in order to allow for MW irradiation. The OLED sample was fabricated on a rectangular glass template of dimensions 44×10 mm^2 with the active area at the center and aligned with the waveguide and a fiberglass spacer with a spring-loaded gold contact plate to keep it in place and provide the electrical contact. Figure 2(b) shows the assembled sample holder mounted to the corrugated waveguide of the spectrometer. The sample [cf. Fig. 2(c)] has lithographically defined indium tin oxide thin-film wiring which defines the OLED back contact and the contact pads. A layer of hard-baked photoresist with apertures serves as an electrical insulator and defines the circular OLED pixel with a diameter of 2 mm. Figure 2(d) shows the lateral and vertical OLED structures: A layer of poly(3,4-ethylenedioxythiophene) polystyrene sulfonate (PEDOT:PSS) serves as a hole injector, and a layer of MEH-PPV constitutes the active device. Layers of Ca and Al form electron injection layers and electrical interconnects to the contact pads, respectively. The device structure is analogous to that described in Ref. [22] with a geometrical arrangement which is more suitable for this particular application where the sample is irradiated with millimeter waves.

The results of amplitude-modulated high-field EDMR experiments are summarized in Figs. 3 and 4. For these
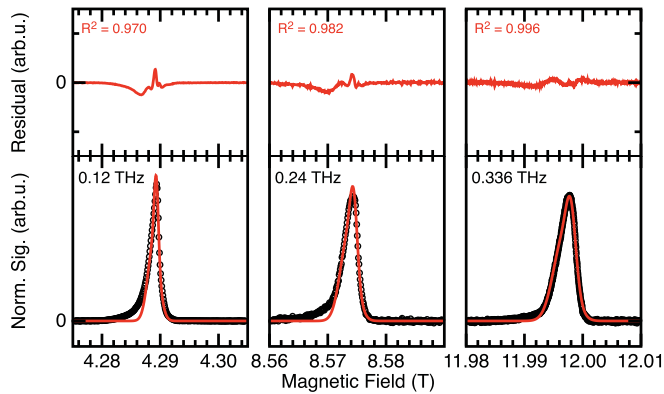
FIG. 3. Lower panels: EDMR spectra at MW frequencies of 120, 240, and 336 GHz along with a global fit to a double-Gaussian model with frequency-dependent broadening. Upper panels: residuals along with coefficients of determination.
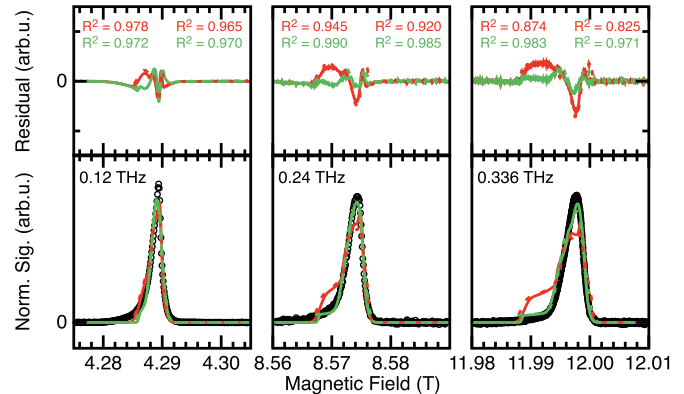

FIG. 4. Measured and simulated spectra. The red lines represent simulations based on DFT where the narrow linewidth is assigned to the electron and the broad linewidth is assigned to the hole. The green lines show opposite assignment. The solid lines correspond to a geometry where the substituents are located on alternating sides of each monomer unit, whereas the dashed lines show the all-*trans* conformation.

experiments, a forward bias of 3.5 V was applied to the sample to give a 20 μA current. The EDMR spectra show resonance peaks with substantially broadened line shapes and strong deviations from the symmetric double-Gaussian line which is characteristic of the EDMR experiments at lower MW frequencies [20]. In Fig. 3, the measured spectra are shown along with a least-squares fit to a global model which assumes a linewidth for each of the two charge carriers $\sigma = \sqrt{\Delta B_{hyp}^2 + \alpha^2 B_0^2}$, a geometric sum of a constant term (B_0-independent hyperfine-fields ΔB_{hyp}), and a broadening term scaling linearly with B_0 [43]. This so-called g-strain broadening assumes a Gaussian distribution of g-factors due to molecular structural disorder which modifies the strength of SOC across the sample. This broadening is isotropic and is described by a B_0-dependent Gaussian linewidth contribution αB_0 (with α as a dimensionless scaling parameter) as described in Ref. [20] and the Supplemental Material [29]. Differences in the g-factors of electrons and holes correspond to an offset between the centers of the two Gaussian lines which scales linearly with B_0. Although such an asymmetry of resonance line centers is not observed at frequencies of < 20 GHz where the linewidth dominated by hyperfine fields [20] exceeds by far any offset induced by differences in g-factor between the resonance lines, it may play a role in the high-field regime.

Using this global model to fit the measured spectra together with the 1.15 GHz spectrum [cf. Fig. 1(a)] we obtain line shapes which describe all three high-field spectra to a certain extent. The free global parameters in this fit are the g-factors of both charge carriers, the two constant linewidths, and the two field-dependent broadening terms α [20]. The upper panels in Fig. 3 show the residuals of this fit along with coefficients of determination. From this least-squares fit we obtain the parameters for the two charge carriers $g_1 = 2.002\,680 \pm 0.000\,005$, $\Delta B_{hyp,1} = 0.2080 \pm 0.0008$ mT, $\alpha_1 = (6.735 \pm 0.044) \times 10^{-5}$ for the narrow resonance and $g_2 = 2.002\,906 \pm 0.000\,005$, $\Delta B_{hyp,2} = 0.8111 \pm 0.0027$ mT, $\alpha_2 = (1.258 \pm 0.008) \times 10^{-4}$ for the wider line. Details of the fitting procedure and the estimates of confidence limits are discussed in the Supplemental Material [29]. The respective hyperfine-field linewidth contributions ΔB_{hyp} are determined by the low-frequency spectrum in Fig. 1(a), and although they are similar to the ones

given in Ref. [20], they lie outside of the stated 95% parameter confidence interval. More significantly, the values for the SOC-induced broadening parameter α are much smaller than those previously extrapolated in Ref. [20] from measurements at smaller B_0 (α_1 and α_2 are reduced by approximately 60% and 75%, respectively). Thus, from the fit results in Fig. 3, we conclude that the simple global model of a double-Gaussian line shape yields only limited agreement with the data. Furthermore, the data substantially contradict the frequency dependence of the linewidths determined in Ref. [20] where it was assumed that SOC leads to isotropic broadening with a linewidth term that scales linearly with B_0. We conclude that, although for the magnetic-field domain below 700 mT studied in Ref. [20] this simple model is sufficient, i.e., it is well suited for the accurate determination of hyperfine-field distributions of the two charge-carrier types, the assumption of isotropic g-tensors (i.e., the applicability of scalar g-factors) is insufficient at higher magnetic fields where SOC contributes to the spectrum.

An appropriate description of the spectra at all frequencies can only be made by performing DFT calculations to assess the g-factor anisotropy. We use the calculated g-tensors (see the Supplemental Material [29]) together with the constant isotropic linewidths and peak-area ratios obtained in the low-field regime [cf. Fig. 1(a)] to simulate the spectrum using the EASYSPIN toolbox [44]. The results of this procedure along with the spectra are shown in Fig. 4. The red lines correspond to cases where the narrow hyperfine distribution [0.5 mT FWHM, cf. Fig. 1(a)] is assigned to the electron and the broad distribution (1.9 mT FWHM) to the hole. The green curves describe the opposite case. In addition to this distinction, the g-tensors are calculated separately for different molecular geometries, i.e., the orientation of the side chain substituents of MEH-PPV is considered. The solid curves correspond to a polymer geometry where the side groups are located on alternating sides for each monomer unit, whereas the dashed lines are computed for an arrangement with all chains lying in parallel, the all-*trans* configuration [cf. Figs. 1(b) and 1(c)].

We emphasize that these simulated spectra are fitted to the experimental data merely by adjustment of a linear vertical scaling factor to compensate for the arbitrary signal amplitude and a horizontal offset to account for absolute measurement error in B_0 at high magnetic fields. The anisotropic line shape is purely a result of the computed g-tensor anisotropy and the experimentally determined hyperfine-field linewidths. The upper panels in Fig. 4 show the fit residuals of the different models along with the coefficients of determination of each curve [45]. The green curves are in good agreement with the measurements, and the overall linewidth and shape are reproduced for all MW frequencies. In contrast, the red curves deviate substantially for higher MW frequencies. The simulated line is much broader than the experimental result and exhibits a bifurcation which is not observed in experiment. The simulation therefore indicates that the green line resembles the physical reality more closely than the red line: The narrow hyperfine distribution is therefore experienced by the hole spin and the broad distribution by the electron. In other words, the hole spin is less strongly hyperfine coupled than the electron spin; the hole wave function is therefore more delocalized while exhibiting a larger g-factor shift due to SOC. The individual line-shape constituents are discussed in more detail in the Supplemental Material [29].

The differences between the solid and the dashed curves in Fig. 4 are not very pronounced, implying that *cis-trans* isomerization has little influence on SOC (the Supplemental Material [29] also shows the small variation of the g-tensor values as a result of changes in molecular geometry). The coefficients of determination for the dashed spectra [all side chains parallel, cf. Figs. 1(b) and 1(c)], stated in the figure, are marginally better than for the solid curves. These two situations represent extreme cases of molecular ordering, and a disordered arrangement of the monomers is much more realistic. No further frequency-dependent broadening mechanisms, such as those due to material inhomogeneity and disorder as discussed in the model in Ref. [20], are taken into account here. Temporal fluctuations of the g-tensors due to molecular dynamics would lead to an even stronger frequency-dependent broadening, and the fact that the experimentally observed linewidths are in such good agreement with the DFT-based simulation indicates that this effect, although conceivable, must be small.

From the comparison of the measured and calculated EDMR spectra we conclude that the computed polaron molecular orbitals and g-tensors provide an accurate description of the physical reality and, even though the simulation is only based on noninteracting segments of four monomer units, this approximation is basically applicable to device operating conditions of the thin films. High-field EDMR therefore offers a unique probe of the polaron wave functions in organic semiconductors, demonstrating that these are truly monomolecular in nature: There is no significant delocalization of the wave function, and intermolecular packing does not appear to influence the g-tensor. We also note that we can exclude the influence of any further resonant paramagnetic species. Although it is possible that charge trapping states can influence steady-state magnetic-field effects, such as magnetoresistance [46,47], such states would appear in the resonance spectrum. However, in this case, we would not be able to find such a high level of agreement between the calculated g-tensors and the measured spectra since trap states were not explicitly considered in the calculation. Our observation that electrons in MEH-PPV experience stronger random hyperfine fields compared to holes confirms a previously expressed hypothesis based on EDMR spectroscopy of electron-acceptor interface processes in bulk heterojunctions [48,49]. In addition, our results suggest that structural disorder has only limited influence on the intermolecular distribution of the magnitude of SOC, a conclusion in agreement with recent qualitative results on the conjugated polymer polyfluorene, a polymer which exists in two distinct structural phases [50]. These results clearly imply that magnetoresistive and magneto-optical effects in MEH-PPV due to the distribution in g-factors will only become relevant at high fields [51]. We conclude that high-field EDMR offers a powerful route to quantifying the influence of SOC. Given the sensitivity of the technique to small perturbations of SOC, this spectroscopy can be used to derive fundamental correlations between molecular structure and SOC. Such correlations are particularly important in unraveling the trade-off between enhanced radiative and nonradiative decay by SOC in phosphorescent OLED emitters [52]. Another exciting possibility would be to attempt to reversibly switch SOC—by electric fields or photo- or electrothermal conformational or electronic perturbations—and monitor this with EDMR. This approach is not limited to organic semiconductors but should also be applicable to other systems, such as molecular magnets.

[1] S. Liang, R. Geng, B. Yang, W. Zhao, R. C. Subedi, X. Li, X. Han, and T. D. Nguyen, Sci. Rep. **6**, 19461 (2016).

[2] Z. G. Yu, Phys. Rev. B **85**, 115201 (2012).

[3] H. Uoyama, K. Goushi, K. Shizu, H. Nomura, and C. Adachi, Nature (London) **492**, 234 (2012).

[4] Z. G. Yu, Phys. Rev. Lett. **106**, 106602 (2011).

[5] W. Barford, R. J. Bursill, and D. V. Makhov, Phys. Rev. B **81**, 035206 (2010).

[6] J. Rybicki and M. Wohlgenannt, Phys. Rev. B **79**, 153202 (2009).

[7] D. S. McClure, J. Chem. Phys. **20**, 682 (1952).

[8] T. Yago, A. Hamasaki, M. Tanaka, T. Takamasu, and M. Wakasa, J. Phys. Chem. C **115**, 21063 (2011).

[9] D. Beljonne, Z. Shuai, G. Pourtois, and J. L. Bredas, J. Phys. Chem. A **105**, 3899 (2001).

[10] M. Wakasa, K. Nishizawa, H. Abe, G. Kido, and H. Hayashi, J. Am. Chem. Soc. **121**, 9191 (1999).

[11] A. J. Schellekens, W. Wagemans, S. P. Kersten, P. A. Bobbert, and B. Koopmans, Phys. Rev. B **84**, 075204 (2011).

[12] V. S. Gladkikh and A. I. Burshtein, J. Phys. Chem. A **110**, 3364 (2006).

[13] L. Nuccio, M. Willis, L. Schulz, S. Fratini, F. Messina, M. D'Amico, F. L. Pratt, J. S. Lord, I. McKenzie, M. Loth, B. Purushothaman, J. Anthony, M. Heeney, R. M. Wilson, I. Hernández, M. Cannas, K. Sedlak, T. Kreouzis, W. P. Gillin, C. Bernhard, and A. J. Drew, Phys. Rev. Lett. **110**, 216602 (2013).

[14] M. Kavand, C. Zhang, D. Sun, H. Malissa, Z. V. Vardeny, and C. Boehme, Phys. Rev. B **95**, 161406(R) (2017).

[15] D. Sun, K. J. van Schooten, M. Kavand, H. Malissa, C. Zhang, M. Groesbeck, C. Boehme, and Z. Valy Vardeny, Nat. Mater. **15**, 863 (2016).

[16] Z. G. Yu, Phys. Rev. Lett. **115**, 026601 (2015).

[17] K. Ando, S. Watanabe, S. Mooser, E. Saitoh, and H. Sirringhaus, Nat. Mater. **12**, 622 (2013).

[18] S. Schott, E. R. McNellis, C. B. Nielsen, H.-Y. Chen, S. Watanabe, H. Tanaka, I. McCulloch, K. Takimiya, J. Sinova, and H. Sirringhaus, Nat. Commun. **8**, 15200 (2017).

[19] B. G. Segal, M. Kaplan, and G. K. Fraenkel, J. Chem. Phys. **43**, 4191 (1965).

[20] G. Joshi, R. Miller, L. Ogden, M. Kavand, S. Jamali, K. Ambal, S. Venkatesh, D. Schurig, H. Malissa, J. M. Lupton, and C. Boehme, Appl. Phys. Lett. **109**, 103303 (2016).

[21] W. J. Baker, K. Ambal, D. P. Waters, R. Baarda, H. Morishita, K. van Schooten, D. R. McCamey, J. M. Lupton, and C. Boehme, Nat. Commun. **3**, 898 (2012).

[22] D. R. McCamey, H. A. Seipel, S.-Y. Paik, M. J. Walter, N. J. Borys, J. M. Lupton, and C. Boehme, Nat. Mater. **7**, 723 (2008).

[23] D. P. Waters, G. Joshi, M. Kavand, M. E. Limes, H. Malissa, P. L. Burn, J. M. Lupton, and C. Boehme, Nat. Phys. **11**, 910 (2015).

[24] H. Malissa, M. Kavand, D. P. Waters, K. J. van Schooten, P. L. Burn, Z. V. Vardeny, B. Saam, J. M. Lupton, and C. Boehme, Science **345**, 1487 (2014).

[25] J. van Tol, L.-C. Brunel, and R. J. Wylde, Rev. Sci. Instrum. **76**, 074101 (2005); D. R. McCamey, G. W. Morley, H. A. Seipel, L. C. Brunel, J. van Tol, and C. Boehme, Phys. Rev. B **78**, 045303 (2008).

[26] M. Kavand, D. Baird, K. van Schooten, H. Malissa, J. M. Lupton, and C. Boehme, Phys. Rev. B **94**, 075209 (2016).

[27] K. J. van Schooten, D. L. Baird, M. E. Limes, J. M. Lupton, and C. Boehme, Nat. Commun. **6**, 6688 (2015).

[28] S.-Y. Lee, S. Paik, D. R. McCamey, and C. Boehme, Phys. Rev. B **86**, 115204 (2012).

[29] See Supplemental Material at http://link.aps.org/supplemental/10.1103/PhysRevB.97.161201 for extensive details about the DFT calculations, the EDMR devices, the EDMR measurements, and the line-shape calculations.

[30] M. Fehr, A. Schnegg, B. Rech, K. Lips, O. Astakhov, F. Finger, G. Pfanner, C. Freysoldt, J. Neugebauer, R. Bittl, and C. Teutloff, Phys. Rev. B **84**, 245203 (2011).

[31] S. Grimme, A. Hansen, J. G. Brandenburg, and C. Bannwarth, Chem. Rev. **116**, 5105 (2016).

[32] S. Grimme, S. Ehrlich, and L. Goerigk, J. Comput. Chem. **32**, 1456 (2011).

[33] S. Grimme, J. Antony, S. Ehrlich, and H. Krieg, J. Chem. Phys. **132**, 154104 (2010).

[34] S. Grimme, J. Antony, T. Schwabe, and C. Muck-Lichtenfeld, Org. Biomol. Chem. **5**, 741 (2007).

[35] F. Weigend and R. Ahlrichs, Phys. Chem. Chem. Phys. **7**, 3297 (2005).

[36] V. N. Staroverov, G. E. Scuseria, J. Tao, and J. P. Perdew, J. Chem. Phys. **119**, 12129 (2003).

[37] TURBOMOLE V7.1 2016, a development of University of Karlsruhe and Forschungszentrum Karlsruhe GmbH, 1989-2007, TURBOMOLE GmbH, since 2007; available at http://www.turbomole.com.

[38] F. Furche, R. Ahlrichs, C. Hättig, W. Klopper, M. Sierka, and F. Weigend, Wiley Interdiscip. Rev.: Comput. Mol. Sci. **4**, 91 (2014).

[39] J.-C. Chen, H.-C. Wu, C.-J. Chiang, T. Chen, and L. Xing, J. Mater. Chem. C **2**, 4835 (2014).

[40] W. Kutzelnigg, U. Fleischer, and M. Schindler, NMR: Basic Princ. Prog. **23**, 165 (1990).

[41] F. Neese, Wiley Interdiscip. Rev.: Comput. Mol. Sci. **2**, 73 (2012).

[42] Y. Ling, S. Van Mierloo, A. Schnegg, M. Fehr, P. Adriaensens, L. Lutsen, D. Vanderzande, W. Maes, E. Goovaerts, and S. Van Doorslaer, Phys. Chem. Chem. Phys. **16**, 10032 (2014).

[43] Note that the linewidth is defined as the Gaussian root-mean-square width σ rather than the full width at half maximum (FWHM) throughout this Rapid Communication as well as in Ref. [20] unless stated otherwise. σ and the FWHM are related according to FWHM $= 2\sqrt{2 \ln 2}\sigma$. For more details, see the Supplemental Material [29].

[44] S. Stoll and A. Schweiger, J. Magn. Reson. **178**, 42 (2006).

[45] Note that the g-tensors used for the line-shape simulation result from the DFT calculation and not from the least-squares fit. Confidence limits can therefore not be estimated from the line-shape simulation. There is only a limited amount of literature that pertains to the comparison of similar calculations to measurements (cf., for example, Ref. [53]).

[46] M. Cox, M. H. A. Wijnen, G. A. H. Wetzelaer, M. Kemerink, P. W. M. Blom, and B. Koopmans, Phys. Rev. B **90**, 155205 (2014).

[47] M. Cox, E. H. M. van der Heijden, P. Janssen, and B. Koopmans, Phys. Rev. B **89**, 085201 (2014).

[48] H. Matsui, T. Hasegawa, Y. Tokura, M. Hiraoka, and T. Yamada, Phys. Rev. Lett. **100**, 126601 (2008).

[49] J. De Ceuster, E. Goovaerts, A. Bouwen, J. C. Hummelen, and V. Dyakonov, Phys. Rev. B **64**, 195206 (2001).

[50] R. Miller, K. J. van Schooten, H. Malissa, G. Joshi, S. Jamali, J. M. Lupton, and C. Boehme, Phys. Rev. B **94**, 214202 (2016).

[51] J. M. Lupton and C. Boehme, Nat. Mater. **7**, 598 (2008).

[52] W. Ratzke, L. Schmitt, H. Matsuoka, C. Bannwarth, M. Retegan, S. Bange, P. Klemm, F. Neese, S. Grimme, O. Schiemann, J. M. Lupton, and S. Höger, J. Phys. Chem. Lett. **7**, 4802 (2016).

[53] M. Kaupp, C. Remenyi, J. Vaara, O. L. Malkina, and V. G. Malkin, J. Am. Chem. Soc. **124**, 2709 (2002).